Crystal Structure at 1.1 Å Resolution of α-Conotoxin PnIB: Comparison with α-Conotoxins PnIA and GI†

Shu-Hong Hu, John Gehrmann, Paul F. Alewood, David J. Craik, and Jennifer L. Martin*

Centre for Drug Design and Development, University of Queensland, Brisbane, QLD 4072 Australia

Received June 2, 1997; Revised Manuscript Received July 9, 1997⊗

ABSTRACT: Conotoxins are small, cysteine-rich peptides isolated from the venom of *Conus* spp. of predatory marine snails, which selectively target specific receptors and ion channels critical to the functioning of the neuromuscular system. α-Conotoxins PnIA and PnIB are both 16-residue peptides (differing in sequence at only two positions) isolated from the molluscivorous snail *Conus pennaceus*. In contrast to the muscle-selective α-conotoxin GI from *Conus geographus*, PnIA and PnIB block the neuronal nicotinic acetylcholine receptor (nAChR). Here, we describe the crystal structure of PnIB, solved at a resolution of 1.1 Å and phased using the Shake-and-Bake direct methods program. PnIB crystals are orthorhombic and belong to the space group $P2_12_12_1$ with the following unit cell dimensions: $a = 14.6$ Å, $b = 26.1$ Å, and $c = 29.2$ Å. The final refined structure of α-conotoxin PnIB includes all 16 residues plus 23 solvent molecules and has an overall *R*-factor of 14.7% (*R*-free of 15.9%). The crystal structures of the α-conotoxins PnIB and PnIA are solved from different crystal forms, with different solvent contents. Comparison of the structures reveals them to be very similar, showing that the unique backbone and disulfide architecture is not strongly influenced by crystal lattice constraints or solvent interactions. This finding supports the notion that this structural scaffold is a rigid support for the presentation of important functional groups. The structures of PnIB and PnIA differ in their shape and surface charge distribution from that of GI.

Conotoxins are small peptides (typically 10−30 residues) found in the venom of the genus *Conus* of predatory marine snails (*1*). These snails immobilize their prey by using a highly specialized cocktail of peptide toxins. On the basis of their feeding and hunting behavior, they can be divided into three main groups: (a) fish-hunting cone snails (piscivorous), (b) mollusc-hunting cone snails (molluscivorous), and (c) worm-hunting cone snails (vermivorous) (*2*).

There are five main classes of conotoxins: the α-, *ω*-, *μ*-, *δ*-, and *κ*-conotoxins, which are categorized according to their biological activities. The α-conotoxins are antagonists of the nicotinic acetylcholine receptors (nAChRs)[1] (*3*). The *ω*-conotoxins inhibit neuronal calcium channels that control neurotransmitter release at synapses (*4*). The *μ*- and *δ*-conotoxins target different sites on the sodium channel to cause blocking or activation, respectively (*1*, *5*, *6*), and the *κ*-conotoxins inhibit the potassium channel (*7*). These toxins are utilized as research tools in many fields of neurobiology since they are high-affinity ligands for a variety of receptors and ion channels.

The nAChR, the target for α-conotoxins, is a member of the family of ligand-gated ion channels and plays a central role in nerve signal transmission (see ref 8 for a review). The nAChR has been implicated in a variety of neuropsychiatric disorders, including Alzheimer's disease and other dementias (*9*). The organization of the nAChR is complex; it is assembled as a pentamer with varying subunit compositions. For example, the five subunits in the muscle receptor differ between developing [$(2\alpha_1)\beta_1\gamma\delta$] and mature muscle [$(2\alpha_1)\beta_1\gamma\epsilon$] (*8*). The neuronal nAChRs are even more complex, with eight possible subtypes for the α subunit (α_2−α_9) and three possible subtypes for the β subunit (β_2−β_4). Each of the five subunits is predicted to incorporate four hydrophobic transmembrane segments (M1−M4) which form the ion channel (*8*). On binding acetylcholine, the receptor is thought to undergo a conformational change, causing a cation-selective channel to open, thereby depolarizing the postsynaptic membrane (*10*, *11*).

Since cell surface receptor proteins and ion channels are often large and multisubunit complexes, they can be difficult to study by X-ray crystallography or nuclear magnetic resonance spectroscopy. Elucidation of the high-resolution three-dimensional structures of the small and highly selective *Conus* peptides is thus an alternative means of investigating receptor structure by providing information about ligand binding sites on receptors and ion channels.

In this paper, we continue our study into the structures of the nAChR-selective α-conotoxins using X-ray crystallographic techniques. Sequence comparison of several α-conotoxins (Figure 1) reveals a conserved cysteine framework, but variation in the size and sequence of the loops defined by the disulfide connections. The classical α-conotoxins isolated from the fish-hunting species (*Conus geographus*, *Conus magus*, and *Conus striatus*), which target the muscle nAChR subtype, have the consensus sequence XCC-(H/N)PACGXX(Y/F)XC. In contrast, the α-conotoxins PnIA and PnIB isolated from the venom of the molluscivorous snail *Conus pennaceus* (*12*) differ both in sequence and

† This work was supported by the Australian Industry Research and Development Board, AMRAD Operations Pty. Ltd., and the Australian Research Council. D.J.C. is an ARC Senior Research Fellow. J.L.M. is a Queen Elizabeth II Fellow.

* Author to whom correspondence should be addressed. Phone: +61 7 3365 4942. Fax: +61 7 3365 1990. E-mail: J.Martin@mailbox.uq.oz.au.

⊗ Abstract published in *Advance ACS Abstracts,* September 1, 1997.

[1] Abbreviations: nAChR, nicotinic acetylcholine receptor; HPLC, high-performance liquid chromatography; rms, root mean square.

S0006-2960(97)01305-6 CCC: $14.00

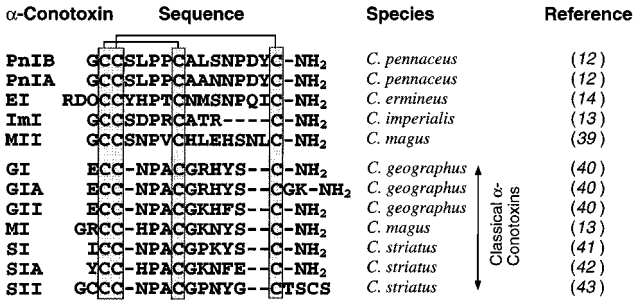

FIGURE 1: Amino acid sequences and conserved cysteine framework (shaded) for the α-conotoxins. The connectivity of the disulfide bonds is shown at the top (note that α-conotoxin SII has an additional disulfide bond, the connectivity of which is not shown). The sequences of the classical α-conotoxins are shown in the lower half of the alignment. NH_2 indicates an amidated C-terminal residue.

in their physiologic effects. Thus, these α-conotoxins are selective for the neuronal rather than the muscle subtype of nAChR and, in addition, are two of the most effective antagonists of neuronal *Aplysia* nAChR (*12*).

Furthermore, the sequences of the *C. pennaceus* α-conotoxins are larger than the classical α-conotoxins (16 residues compared with the usual 13) and do not fit the consensus sequence. Thus, PnIB has the sequence GCCSLPPCAL-SNPDYC-NH_2 (the disulfide linkages are Cys 2−Cys 8 and Cys 3−Cys 16) with four and seven residues in the loops between the cysteines, as opposed to the usual loops of three and five residues. The sequences of PnIA and PnIB differ at two positions, with Leu 10 and Ser 11 in PnIB replacing Ala 10 and Asn 11 of PnIA. Interestingly, the sequences of the α-conotoxins ImI from the worm-hunting *Conus imperialis*, which targets the neuronal nAChR (*13*), and EI from the fish-hunting *Conus ermineus* (*14*) also diverge in sequence from those of the classical α-conotoxins from fish-hunting species.

To date, there is very little structural information for the α-conotoxins. The crystal structures of α-conotoxins PnIA (*15*) and GI (*16*) from *C. geographus* were solved by direct methods at 1.1 and 1.2 Å, respectively. In addition, the solution structures of GI (*17*) and of the unusual αA-conotoxin PIVA from *Conus purpurascens* (*18*), which has three disulfide bonds rather than the usual two, have been determined by NMR. Here, we report the 1.1 Å crystal structure of synthetic α-conotoxin PnIB and compare it with the crystal structures of the related neuronal nAChR-selective α-conotoxin PnIA and with the muscle subtype-selective nAChR antagonist α-conotoxin GI.

MATERIALS AND METHODS

Peptide Synthesis, Crystallization, and Data Collection. The α-conotoxin PnIB was synthesized and purified using the protocol previously described for α-conotoxin PnIA (*15*). The purity of the peptide was checked by analytical reverse-phase HPLC and mass spectrometry. Crystallization experiments were performed in a manner similar to that for PnIA (*15*). Crystals of PnIB were grown from macro-seeded (*19*) hanging drops at 14 °C by combining 2 μL of 5 mg/mL PnIB, dissolved in deionized water, with 2 μL of reservoir solution containing 1.0 M sodium formate. The crystals of PnIB belong to space group $P2_12_12_1$ with the following unit cell dimensions: $a = 14.6$ Å, $b = 26.1$ Å, and $c = 29.2$ Å. Assuming one molecule per asymmetric unit, the crystal volume per unit of molecular mass (V_m) is 1.61 Å^3 Da^{-1} with a solvent content of 24%, which is lower than the normal range (30−70%) observed for protein crystals (*20*) but twice that observed for crystals of α-conotoxin PnIA (*15*).

Table 1: X-ray Data and Refinement Statistics

	Diffraction Data		
	crystal 1	crystal 2	merged data
maximal resolution (Å)	1.1	1.1	1.1
no. of observations	17 040	22 601	39 641
no. of unique reflections	4008	4321	4483
all data			
completeness (%)	78.7	88.2	91.5
R_{sym}[a]	0.067	0.075	0.080
1.1−1.14 Å			
completeness (%)	32.1	69.7	73.8
R_{sym}[a]	0.303	0.287	0.311

	Structure Refinement	
	$F > 2\sigma F$ cutoff	all data
resolution range (Å)	6.0−1.1	20−1.1
no. of reflections	3370	4365
isotropic		
R-factor[b]	0.147	0.176
R-free[c]	0.157	0.189
anisotropic		
R-factor[b]	0.132	
R-free[c]	0.160	
no. of peptide atoms	113	
no. of solvent atoms	23	
rms bond length (Å)	0.006	
rms bond angles (deg)	1.7	
rms dihedral angles (deg)	22.0	
rms improper angles (deg)	1.5	
overall *B*-factor (Å^2)		
all atoms	7.5	
main chain atoms	6.4	
side chain atoms	8.6	
solvent atoms	27	

[a] $R_{sym} = \sum|I-\langle I\rangle|/\sum\langle I\rangle$. [b] R-factor $= \sum|F_{obs}-F_{calc}|/\sum F_{obs}$. [c] R-free as defined by Brünger (*38*).

Data to 1.1 Å were measured at 16 °C on an *R*-axis IIC imaging plate area detector system mounted on a Rigaku RU-200 copper rotating anode X-ray source, operating at 46 kV and 60 mA (Yale double-focusing mirror monochromator, 0.2 mm cathode, and 0.5 mm collimator). The crystal to detector distance was 93 mm, and a swing angle (2θ) of 44° was used. Data were measured from two crystals, using two different orientations of each to maximize data completeness. The intensity data were processed using the programs DENZO and SCALEPACK (*21*, *22*). The merged data set consists of 39 641 observations corresponding to 4483 unique reflections. The data are 91.5% complete to 1.1 Å, and the overall merging $R_{sym}(I)$ is 8.0%. Crystallographic statistics for data collection are shown in Table 1.

Structure Determination and Refinement. Using the crystal structure of PnIA as a search model, no clear solution was found in rotation function searches in XPLOR (*23*) or MERLOT (*24*). Instead, the positions of the four sulfur atoms of PnIB were determined by direct methods using the program Shake-and-Bake (*25*). Normalized structure-factor magnitudes ($|E|$'s) were calculated with the program BAYES, LEVY, and EVAL (*26*). About 100 trial structures were generated using 200 cycles of the Shake-and-Bake procedure per randomly generated trial structure. A histogram of the $R(\varphi)$ values showed a bimodal distribution with two solutions from the 100 trials in the range of 0.388−0.391. The two

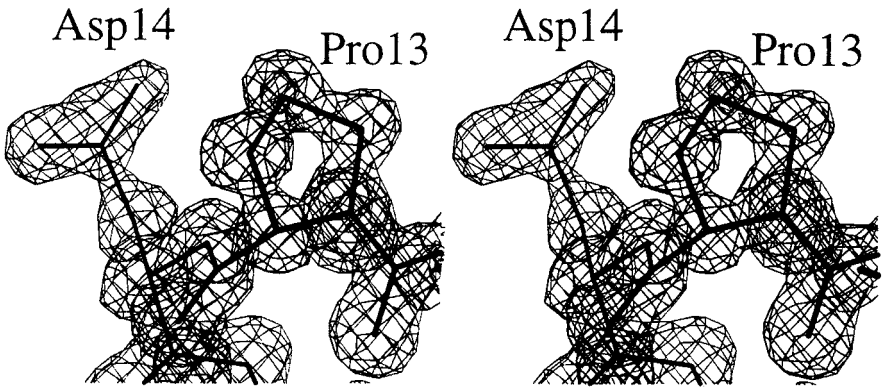

FIGURE 2: $2F_o - F_c$ electron density for the region around residues Pro 13 and Asp 14 of α-conotoxin PnIB, contoured at 1σ.

solutions with the lowest $R(\varphi)$ values clearly revealed the four highest peaks as the two disulfide bridges of the molecule.

The four sulfur atoms of PnIB identified by Shake-and-Bake were then superimposed onto the corresponding sulfurs of the PnIA crystal structure (*15*) using INSIGHT II (TMSI). The root mean square (rms) deviation for the four S atoms was 0.16 Å. The initial crystallographic *R*-factor for the manually rotated and translated PnIA model of PnIB was 42.9%, with an *R*-free (calculated from 10% of the data) of 45.9%. The two residues which differ in sequence between PnIA and PnIB were initially modeled as alanine. The model was first refined by rigid body refinement using X-PLOR 3.1 (*23*). $2F_o - F_c$ and $F_o - F_c$ electron density maps showed side chain density for both these residues, Leu 10 and Ser 11, and these side chains were subsequently built into the structure. Several rounds of model building in O (*27*) and positional and individual *B*-factor refinement with X-PLOR, using Engh and Huber geometrical parameters (*28*), gave an *R*-factor of 22.2% with an *R*-free of 23.6% at 1.5 Å resolution. The resolution of the data was gradually increased to 1.1 Å, and alternative side chain conformations were modeled for Ser 4 and Ser 11. Water molecules were included where difference electron density showed a peak above 3σ, and the modeled water made stereochemically reasonable hydrogen bonds. A final round of X-PLOR positional and individual isotropic *B*-factor refinement for all 16 residues and 23 water molecules gave an *R*-factor of 14.7% and an *R*-free of 15.7% for all data with structure-factor amplitudes of $F > 2\sigma F$ between 6.0 and 1.1 Å. SHELXL93 (*29*) was used for anisotropic *B*-factor refinement, giving an *R*-factor of 13.2% with an *R*-free of 16.0% using the same data. Statistics for the final refined structure are shown in Table 1. The quality and geometry of the model were evaluated by PROCHECK (*30*). Coordinates and structure factors for α-conotoxin PnIB have been deposited with the Brookhaven Protein Data Bank (accession code 1AKG), and both will be on hold for 1 year.

The structures of α-conotoxin GI (PDB accession code 1NOT) (*16*) and PnIA (PDB accession code 1PEN) (*15*) were used for structural comparison with PnIB. Programs used for analyses and comparisons included O (*27*), GRASP (*31*), INSIGHT (TMSI), and MOLSCRIPT (*32*). Figures for this paper were generated using these programs.

RESULTS

Structure Determination and Quality of the Model. Despite a sequence difference of only two of 16 residues, PnIB crystallizes under quite different conditions to PnIA and grows in the orthorhombic space group $P2_12_12_1$, whereas PnIA was crystallized in the monoclinic space group $P2_1$. Furthermore, the solvent content of the PnIB and PnIA crystals is significantly different, with a theoretical solvent content of 24% in the PnIB crystals compared with only 12% in the PnIA crystals. The difference in the crystal forms of PnIA and PnIB is fortuitous since it allows us to analyze the robustness of this α-conotoxin fold, that is, to investigate whether the unusual fold of α-conotoxin PnIA is conserved in PnIB under different crystal lattice constraints.

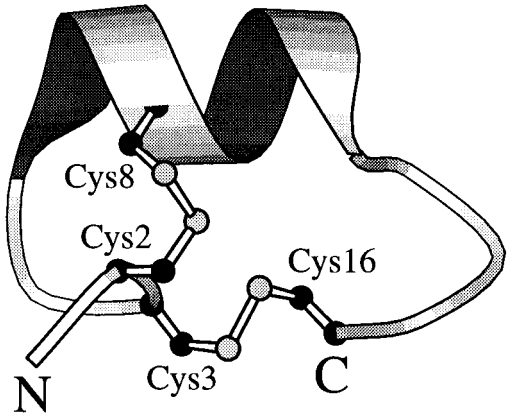

FIGURE 3: Ribbon representation of the α-conotoxin PnIB structure with the two disulfide bonds shown in a ball-and-stick representation. This figure was produced using MOLSCRIPT (*32*).

The $2F_o - F_c$ electron density map is well-defined for all atoms of PnIB (see, for example, Figure 2). The final refined structure of PnIB (Figure 3) is comprised of all 16 residues in the sequence and 23 solvent molecules, a total of 136 atoms, and has excellent crystallographic statistics (Table 1). Two alternate conformations are observed for Ser 4 and Ser 11. Analysis of the Ramachandran plot (data not shown) reveals that the ϕ and ψ backbone dihedrals of all residues of PnIB fall in the allowed regions. The mean coordinate error of the structure is estimated to be 0.1−0.2 Å, based on Luzzati plot analysis of *R*-factor and *R*-free values (*33*). The quality of the model is revealed in the low average isotropic *B*-factors for main chain and side chain atoms of 6.4 and 8.6 Å^2, respectively (7.4 and 9.2 Å^2 for anisotropic *B*-factors, respectively).

Structure of PnIB and Comparison with PnIA. The main feature of the α-conotoxin PnIB structure is the α-helical region (two turns of helix) formed by residues 5−12. In addition, residues 2−4 form a 3_{10}-helical turn, and the C-terminal residues are involved in two consecutive β-turns

Table 2: Hydrogen Bond Interactions in PnIB

contact		distance (Å)	contact		distance (Å)
intramolecular			PnIB−water		
Gly 1 O	Ser 4 N	3.1	Ala 9 O	Wat 27	2.7
Gly 1 O	Ser 4 Oγ^a	3.0	Leu 10 O	Wat 22(3)	2.8
Cys 2 O	Ser 4 N	3.2	Ser 11 O	Wat 28(1)	2.9
Cys 2 O	Leu 5 N	3.1	Ser 11 Oγ	Wat 33	2.6
Cys 2 O	Ala 9 N	3.4	Ser 11 Oγ	Wat 36	2.7
Ser 4 Oγ^a	Gly 1 N	3.3	Ser 11 Oγ^a	Wat 19	2.5
Leu 5 O	Cys 8 N	2.9	Asn 12 Nδ2	Wat 19(4)	2.9
Leu 5 O	Ala 9 N	3.0	Asn 12 Oδ1	Wat 21(4)	2.7
Pro 6 O	Ala 9 N	3.3	Pro 13 O	Wat 26	2.7
Pro 6 O	Leu 10 N	3.0	Asp 14 N	Wat 34	3.2
Pro 7 O	Ser 11 Oγ	3.3	Asp 14 O	Wat 29	2.8
Pro 7 O	Ser 11 Oγ^a	3.1	Asp 14 O	Wat 30	2.8
Pro 7 O	Ser 11 N	3.4	Asp 14 Oδ1	Wat 31	2.8
Pro 7 O	Ser 11 N	3.1	Asp 14 Oδ1	Wat 35	2.7
Cys 8 O	Ser 11 Oγ^a	3.0	Tyr 15 N	Wat 34	3.1
Cys 8 O	Asn 12 N	3.0	Tyr 15 O	Wat 29	2.9
Cys 8 O	Asn 12 Nδ2	2.9	Tyr 15 Oη	Wat 19	2.6
Ala 9 O	Asn 12 N	3.2	Tyr 15 Oη	Wat 38(4)	2.6
Ser 11 Oγ^a	Asn 12 Nδ2	3.2	Cys 16 O	Wat 19(4)	2.5
Asn 12 O	Tyr 15 N	3.4	water−water		
Asn 12 O	Cys 16 N	3.1	Wat 17	Wat 35	3.4
intermolecular^b			Wat 17	Wat 23(3)	2.8
Cys 2 N	Asn 12 Oδ1(4)	3.3	Wat 17	Wat 24(3)	3.1
Cys 2 N	Cys 16 O(4)	2.8	Wat 18	Wat 36(1)	2.7
Cys 3 N	Asn 12 Oδ1(4)	3.0	Wat 18	Wat 38(1)	2.4
PnIB−water			Wat 20	Wat 28(4)	2.8
Gly 1 N	Wat 20	3.2	Wat 20	Wat 30(4)	2.6
Gly 1 N	Wat 21	2.8	Wat 21	Wat 34(4)	2.8
Gly 1 N	Wat 32	3.2	Wat 22	Wat 23	2.8
Gly 1 O	Wat 29(4)	3.2	Wat 23	Wat 24	3.1
Cys 3 O	Wat 18	2.7	Wat 23	Wat 38(1)	2.8
Cys 3 O	Wat 24	3.1	Wat 24	Wat 35(3)	2.7
Cys 3 O	Wat 38(1)	3.4	Wat 25	Wat 37(2)	2.7
Ser 4 O	Wat 26(3)	2.9	Wat 25	Wat 35(3)	2.8
Ser 4 O	Wat 27(4)	2.8	Wat 25	Wat 39(3)	2.9
Ser 4 Oγ	Wat 21	2.7	Wat 26	Wat 27	2.7
Ser 4 Oγ	Wat 22	2.9	Wat 26	Wat 36(1)	2.8
Ser 4 Oγ^a	Wat 21	2.6	Wat 27	Wat 39(3)	2.8
Ser 4 Oγ^a	Wat 39	3.3	Wat 29	Wat 32	2.9
Pro 6 O	Wat 25	2.9	Wat 30	Wat 31	2.8
Pro 7 O	Wat 33	2.8	Wat 31	Wat 37	2.9
Pro 7 O	Wat 38	3.3	Wat 33	Wat 38	2.9

^{a} Alternate conformations. ^{b} (1)−(4) correspond to different symmetry elements: (1) x, y, z; (2) $^1/_2 - x, -y, ^1/_2 + z$; (3) $-x, ^1/_2 + y, ^1/_2 - z$; and (4) $^1/_2 + x, ^1/_2 - y, -z$.

(type I, residues 12−15; type IV, residues 13−16). The structure is constrained by two disulfide bridges linking Cys 2 and Cys 8 and Cys 3 and Cys 16 and is further stabilized by 21 intramolecular, 3 intermolecular, and 35 water-associated hydrogen bonds (Table 2). Most of the intramolecular hydrogen bonds are associated with main chain stabilization of secondary structure elements and are also observed in the PnIA structure. In addition, hydrogen bonds are formed intramolecularly between the Ser 4 side chain and Gly 1 main chain, between the Ser 11 side chain and Pro 7 and Cys 8 main chains, between the Asn 12 side chain and Cys 8 main chain, and between the Asn 12 and Ser 11 side chains.

Overall, the structure of PnIB is very similar to that of PnIA (*15*), as shown schematically in Figure 4, in which the two structures are superimposed. The backbones of the two α-conotoxins superimpose very well, and the side chains are similar in most cases. The ϕ and ψ main chain angles for each residue in PnIB and PnIA are listed in Table 3, showing that the backbone conformations are similar (these angles vary by less than 10° for most of the 16 residues). The largest differences in main chain angles between PnIB and PnIA are ∼20° for Pro 13 and Tyr 15. The main chain atoms of the two structures can be superimposed with an rms deviation of 0.36 Å. The largest deviation in Cα positions between PnIB and PnIA is for residue Asp 14, which differ between the two structures by 0.92 Å. All other Cα atoms of PnIB and PnIA are within 0.35 Å. Furthermore, the side chain positions of PnIB and PnIA are also very similar, with the largest differences occurring at Asp 14 and Tyr 15 (Figure 4). The electron density for this region of the PnIB structure is very good (Figure 2), showing that the structural differences in PnIB do not arise from a poorly defined part of the structural model.

The side chain of Asp 14 is observed in a gauche+ conformation in PnIB (χ^1 of −61°, χ^2 of −59°) and a gauche− conformation in PnIA (χ^1 of 51°, χ^2 of −30°). The side chain conformation of Asp 14 in PnIA is stabilized by an intermolecular hydrogen bond with a neighboring molecule (Asp 14 Oδ2−Cys 2 N, 2.8 Å). By comparison, the side chain of Asp 14 of PnIB interacts only with solvent molecules. The solvent accessibility (using a probe radius of 1.4 Å) of the Asp 14 side chain in PnIB is 25% greater than that of PnIA (120 and 94 Å^2, respectively). Accord-

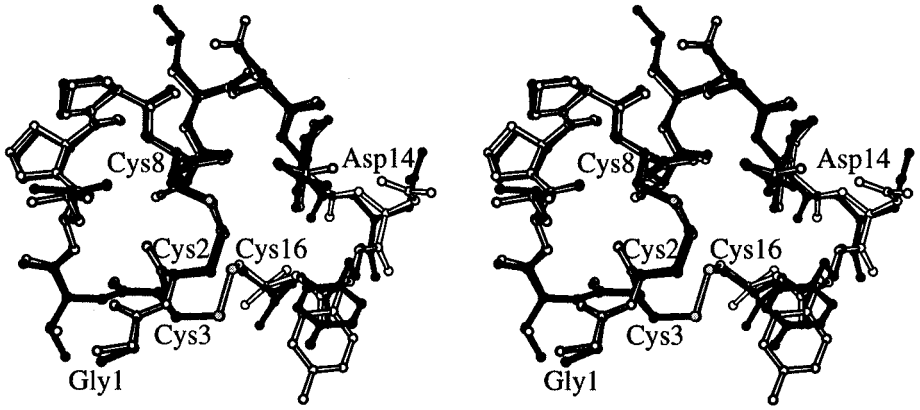

FIGURE 4: Stereo superimposition of the structures of α-conotoxins PnIB (black) and PnIA (white). This figure was produced using MOLSCRIPT (*32*).

Table 3: Main Chain ϕ and ψ Angles for Each Residue of PnIB (and PnIA)

residue	ϕ (deg)	ψ (deg)
Gly 1	–	–
Cys 2	−50 (−46)	−46 (−53)
Cys 3	−70 (−67)	−12 (−14)
Ser 4	−105 (−102)	4 (−5)
Leu 5	−116 (−104)	104 (112)
Pro 6	−39 (−40)	−53 (−56)
Pro 7	−59 (−60)	−38 (−38)
Cys 8	−74 (−73)	−44 (−46)
Ala 9	−59 (−58)	−38 (−45)
Leu (Ala) 10	−62 (−66)	−39 (−31)
Ser (Asn) 11	−87 (−88)	−8 (−8)
Asn 12	−133 (−135)	57 (58)
Pro 13	−61 (−64)	−44 (−27)
Asp 14	−73 (−65)	−31 (−37)
Tyr 15	−66 (−87)	−46 (−46)
Cys 16	−80 (−80)	−20 (−22)

ingly, the PnIB conformation of Asp 14 may best represent the unhindered conformation of this acidic side chain.

Tyr 15 adopts a trans conformation in both PnIA and PnIB, but there is a 20° difference in the χ^2 dihedral (PnIB, χ^1 of 173° and χ^2 of 85°; PnIA, χ^1 of 177° and χ^2 of 64°). The small difference in conformation of this residue in the two α-conotoxins, again, is probably a result of differing environments. The solvent accessibility of PnIB Tyr 15 is ∼10% less than that of PnIA (137 and 150 Å^2, respectively). A 4 Å cutoff reveals 19 van der Waals intermolecular interactions each for the tyrosine side chain in both α-conotoxins, but Tyr 15 of PnIB makes three short intermolecular contacts (Tyr 15 Cδ1−Ser 4 Oγ, 3.3 Å; Tyr 15 Oη−Cys 8 Cα, 3.4 Å; and Tyr 15 Cϵ2−Cys 8 Sγ, 3.4 Å) compared with only one with the PnIA Tyr 15 side chain (Tyr 15 Cδ1−Cys 8 Sγ, 3.4 Å).

Disulfide Bridges. The conformations of the two disulfide bonds of PnIB, Cys 2−Cys 8 (χ_{ss} = −100.3°) and Cys 3−Cys 16 (χ_{ss} = −91.1°) are similar to those of PnIA, with both belonging to the left-handed spiral type (Table 4), which is the most populated disulfide conformation found in protein structures (*34*, *35*). The distances between the disulfide-bridged cysteine Cα atoms in PnIB are 5.1 Å for Cys 2−Cys 8 and 5.6 Å for Cys 3−Cys 16, which are within the usual range found for proteins. In contrast, the α-conotoxin GI crystal structure (*16*) has one left-handed (Cys 2−Cys 7, χ_{ss} = −91.8°) and one right-handed (Cys 3−Cys 13 χ_{ss} = +97.4°) disulfide bridge.

Solvent Structure. Twenty-three solvent molecules, modeled as water, were built into the PnIB structure, and all are within hydrogen bonding distance of proton donor or acceptor atoms of the α-conotoxin (Table 2). The average temperature or *B*-factor of these modeled water molecules is 27 Å^2. This is somewhat higher than the average *B*-factor of the peptide atoms of α-conotoxin PnIB (7.5 Å^2) but is similar to the average *B*-factor of waters in the crystal structure of α-conotoxin GI (21 waters, average *B*-factor of 28 Å^2). For the crystal structure of α-conotoxin PnIA, which has a lower solvent content of 12 waters, the average *B*-factor of the waters (19 Å^2) is also lower.

Three of the 23 water molecules in PnIB interact with the positively charged N-terminal amine, and two waters interact with the negatively charged side chain of Asp 14. The polar side chains of Ser 4, Ser 11, and Asn 12 each interact with two water molecules, and the phenolic hydroxyl group of Tyr 15 also interacts with two waters. A total of 18 other interactions are observed in the PnIB structure between main chain amide atoms and water molecules. Although the PnIA crystal structure has only 12 waters modeled, a similar number of hydrogen bond interactions are observed for side chain and main chain atoms. However, there is a significant difference in the number of water−water interactions between the two crystal structures. PnIB has 22 (Table 2) and PnIA 10. This observed "looser" packing of the PnIB crystals compared with that of PnIA is consistent with the increased solvent content of PnIB crystals (24%, 23 waters modeled) compared with that of PnIA (12%, 12 waters modeled).

Crystal Packing. This looser packing of PnIB is also apparent in the lower number of intermolecular contacts between symmetry-related molecules compared with the number in PnIA. Using a 4 Å cutoff, there are 63 intermolecular peptide contacts found in the PnIB crystal structure compared with 68 intermolecular contacts in PnIA. Using a much tighter 3.4 Å cutoff, only 10 contacts are found for PnIB compared with 15 for PnIA. In both crystal structures, only three peptide−peptide intermolecular hydrogen bonds are found (Table 2). In PnIB, two of these involve the side chain of Asn 12; the backbone nitrogens of symmetry-related Cys 2 (3.3 Å) and Cys 3 (3.0 Å) form hydrogen bonds with Asn 12 Oδ1. The third intermolecular hydrogen bond is between the backbone oxygen of symmetry-related Cys 16 (2.8 Å) and the amide nitrogen of Cys 2. The three intermolecular hydrogen bonds in the PnIA

Table 4: Disulfide Bridge Conformations in α-Conotoxin Crystal Structures

α-conotoxin	cys 1	cys 2	χ^1 (deg)	χ^2 (deg)	χ (deg)	$\chi^{2'}$ (deg)	$\chi^{1'}$ (deg)	Cα-Cα (Å)	disulfide type
PnIB	Cys 2	Cys 8	−174.5	73.0	−100.3	−88.2	−169.6	5.1	left-hand
	Cys 3	Cys 16	−49.5	−57.1	−91.1	−63.9	−72.0	5.6	left-hand
PnIA	Cys 2	Cys 8	−171.7	70.6	−98.6	−90.4	−163.6	5.0	left-hand
	Cys 3	Cys 16	−48.5	−51.9	−83.1	−62.6	−64.9	5.4	left-hand
GI	Cys 2	Cys 7	−157.5	−64.1	−91.8	−95.0	−68.4	5.9	left-hand
	Cys 3	Cys 13	−66.1	−84.9	97.4	79.8	−167.8	5.0	right-hand

crystal structure are quite different, as might be expected given the different crystal packing arrangement. In PnIA, Asn 12 Oδ1 is stabilized by only one intermolecular contact, to a symmetry-related N-terminal amino group (2.8 Å). The N-terminal amino group forms a hydrogen bond with the main chain carbonyl oxygen of Cys 16 (3.0 Å) from a symmetry-related molecule. In addition, in PnIA, there is a symmetry-related hydrogen bond formed between the backbone nitrogen of Cys 2 and the acidic side chain Oδ2 of Asp 14 (2.8 Å).

Structural Comparison of PnIB and PnIA with GI. What makes α-conotoxins such as GI selective for the muscle nAChR subtype and α-conotoxins such as PnIA and PnIB selective for the neuronal nAChR subtype? PnIA and PnIB are similar in sequence, function, and structure, but they differ in sequence and function with respect to α-conotoxin GI isolated from fish-hunting *C. geographus*. Structural comparison of PnIB and PnIA with the crystal structure of GI (*16*) shows that they also differ in structure. The only sequence similarity between PnIA and PnIB and GI is the conserved cysteine disulfide framework, a conserved proline near the N terminus (Pro 5 in GI and Pro 6 in PnIA and PnIB), and possibly a tyrosine near the C terminus (Tyr 11 in GI and Tyr 15 in PnIA and PnIB). The two inter-cysteine loops are four and seven residues in PnIA and PnIB, compared with three and five residues, respectively, in the α-conotoxin GI. The conformations of PnIB, PnIA, and GI are all established by the two disulfide bonds that form the core of the molecules. In PnIA and PnIB, these disulfides are conformationally equivalent, but one of these is right-handed in GI (Table 4). The disulfide atoms (Cα, Cβ, and Sγ) of PnIB superimpose onto those of GI (Figure 5), with an rms deviation of 1.5 Å. This compares with an rms deviation for the same atoms in PnIB and PnIA of 0.18 Å.

Using this superimposition, the conserved proline residues of PnIB and GI are relatively close in space, with a separation of ∼0.8 Å. However, the aromatic side chains Tyr 11 of GI and Tyr 15 of PnIB are in entirely different spatial relationships, being on opposite sides of the molecular structure and some 7−8 Å distant from each other. Furthermore, Tyr 11 of GI is more tightly packed into the molecular structure than Tyr 15 of PnIB. Thus, the aromatic ring of GI forms 11 van der Waals contacts (4 Å cutoff) with atoms in the core of the conotoxin structure, while the tyrosine rings of PnIB and PnIA form only six and five van der Waals contacts, respectively. The calculated solvent accessibility of the Tyr 11 side chain of GI (108 Å^2, using a probe radius of 1.4 Å) is also less than that of the tyrosines in PnIB and PnIA (131 and 150 Å^2, respectively).

We also compared the shape and surface charge distribution of these α-conotoxin structures (Figure 6). PnIA and PnIB have very similar surfaces and shapes, so the comparison in Figure 6 is only shown for PnIB and GI. Clearly,

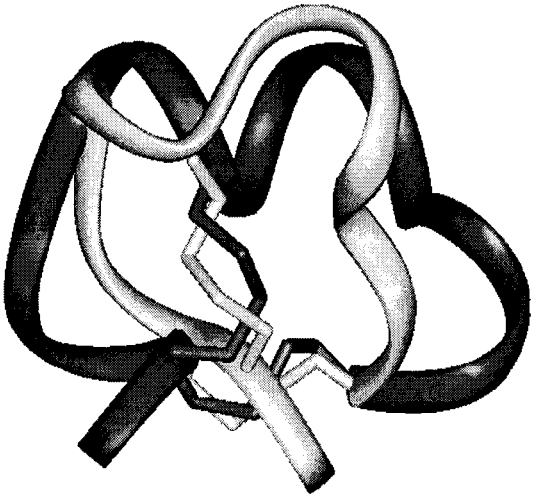

FIGURE 5: Comparison of the α-conotoxin PnIB backbone structure (dark gray) with that of α-conotoxin GI (light gray). The superimposition was produced by overlaying atoms of the two disulfide bonds of both α-conotoxins. This figure was generated using the INSIGHT package (TMSI).

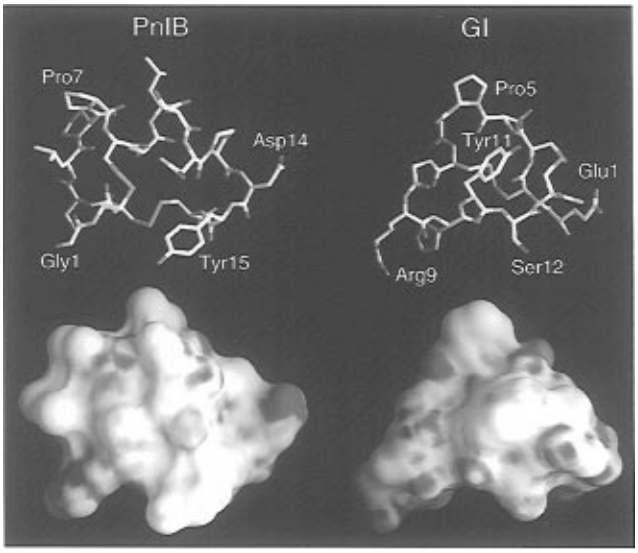

FIGURE 6: Comparison of the molecular structures (top) and molecular shapes and electrostatic surfaces (bottom) of the functionally different α-conotoxins PnIB (left) and GI (right). The molecular structures are colored according to atom type: white for carbon, light blue for nitrogen, red for oxygen, and green for sulfur. The electrostatic surface is colored according to charge: blue for positive, red for negative, and white for hydrophobic regions. Charges are taken from X-PLOR tophcsdx.pro parameters. This figure was generated using GRASP (*31*).

the shapes of the two α-conotoxins are quite different; that of GI has been described as triangular (*16*), while PnIB is rectangular, like that of PnIA (*15*). With regard to surface charge differences in these α-conotoxins, a positively charged residue (arginine or lysine) has been implicated in receptor

binding of the muscle-selective nAChR antagonists (*16*, *17*, *36*). However, arginine and lysine residues are absent in the sequences of the neuronal nAChR-selective antagonists PnIA and PnIB. Indeed, the only charged regions in PnIA and PnIB are the negatively charged Asp 14 side chain and the positively charged amino terminus of Gly 1 (the C-terminal Cys 16 of PnIA and PnIB is amidated), giving a net charge of zero. In PnIB, these two charged regions are located at opposite ends of the rectangular molecule, separated by 16 Å [this is similar to PnIA (*15*)]. Conversely, GI has a net charge of +1, with a negatively charged residue (Glu 1) at the positively charged N terminus and a positively charged residue (Arg 9) close to the C terminus. In Figure 6, the GI surface is oriented to optimize the match of charge distribution with PnIB without regard to any underlying molecular superimposition or sequence alignment. Even after the surfaces are matched in this way, it is clear that the surface charge is quite different for these two α-conotoxins.

DISCUSSION

Three α-conotoxin crystal structures have now been determined: GI (*16*), PnIA (*15*), and now PnIB. All three structures were determined by Shake-and-Bake direct methods (*25*, *37*), showing that it is a generally applicable method for solving crystal structures of this class. We have found, that for α-conotoxin structures, the important requirement for structure determination by this method is the availability of high-resolution data. In these structures, the presence of four sulfur atoms out of 120−130 atoms in the asymmetric unit allows for very rapid structure determination with Shake-and-Bake. The most difficult aspect of this work is obtaining suitable crystals for high-resolution data measurement. Thus, despite the sequence and functional similarity of PnIB and PnIA, the two α-conotoxins crystallize under different conditions and in different space groups. Examination of the PnIB structure in the PnIA crystal lattice shows that PnIB cannot adopt the same tight crystal packing because of unfavorable interactions between Leu 10 and a symmetry-related molecule.

However, the high-resolution crystal structure of PnIB does show it to have a high degree of structural equivalence with respect to PnIA. The conserved cysteines in the sequences of PnIA and PnIB form exactly equivalent disulfide bonds; these form the core of the conotoxin structure and stabilize a backbone fold that facilitates the surface display of other functional groups. The structural equivalence between PnIA and PnIB is present despite different packing arrangements and a doubling of the percentage solvent content in going from the PnIA to PnIB crystal form, showing that the fold is not significantly modified by crystal contacts. These findings strongly support the notion that this α-conotoxin motif is a rigid scaffold for presentation of specific chemical groups. This type of molecular scaffold could thus be useful as a template in the molecular design of compounds having a wide range of activities.

The structural similarity between the two α-conotoxins PnIB and PnIA is important in understanding their functional similarity as antagonists of neuronal nAChR. Furthermore, the structural and surface differences between PnIB and PnIA and GI, a selective antagonist of muscle subtype nAChR, provide a means of assessing their differing functions. Compared with GI, the structures of PnIB and PnIA have differing disulfide conformations, differing shapes, and differing charge distributions. These results show that a conserved cysteine framework does not necessarily produce a conserved fold if the spacing (number of residues) between the cysteines varies significantly. Also, our results suggest that variations in surface charge and/or molecular shape could be a means of selectively targeting the muscle or neuronal subtypes of nAChR in these α-conotoxins.

ACKNOWLEDGMENT

We thank Luke Guddat, Richard Lewis, and Peter Andrews for many helpful discussions. We are grateful to Alun Jones for mass spectrometric analyses and Ann Atkins, Marion Loughnan, and Trudy Bond for amino acid analyses and sequencing.

REFERENCES

1. Olivera, B. M., Rivier, J., Clark, C., Ramilo, C. A., Corpuz, G. P., Abogadie, F. C., Mena, E. E., Woodward, S. R., Hillyard, D. R., and Cruz, L. J. (1990) *Science 249*, 257−263.
2. Kohn, A. J., and Nybakken, J. W. (1975) *Mar. Biol. (Berlin) 29*, 211−234.
3. Olivera, B. M., McIntosh, J. M., Cruz, L. J., Luque, F. A., and Gray, W. R. (1984) *Biochemistry 23*, 5087−5090.
4. Olivera, B. M., Gray, W. R., Zeikus, R., McIntosh, J. M., Varga, J., Rivier, J., de Santos, V., and Cruz, L. J. (1985) *Science 230*, 1338−1343.
5. Shon, K.-J., Grilley, M. M., Marsh, M., Yoshikami, D., Hall, A. R., Kurz, B., Gray, W. R., Imperial, J. S., Hillyard, D. R., and Olivera, B. M. (1995) *Biochemistry 34*, 4913−4918.
6. Fainzilber, M., Lodder, J. C., Kits, K. S., Kofman, O., Vinnitsky, I., Van Rietschoten, J., Zlotkin, E., and Gordon, D. (1995) *J. Biol. Chem. 270*, 1123−1129.
7. Terlau, H., Shon, K.-J., Grilley, M., Stocker, M., Stühmer, W., and Olivera, B. M. (1996) *Nature 381*, 148−151.
8. Galzi, J.-L., Revah, F., Bessis, A., and Changeux, J.-P. (1991) *Annu. Rev. Pharmacol. 31*, 37−72.
9. Holladay, M. W., Lebold, S. A., and Lin, N.-H. (1995) *Drug Dev. Res. 35*, 191−213.
10. Unwin, N. (1993) *J. Mol. Biol. 229*, 1101−1124.
11. Unwin, N. (1995) *Nature 373*, 37−43.
12. Fainzilber, M., Hasson, A., Oren, R., Burlingame, A. L., Gordon, D., Spira, M. E., and Zlotkin, E. (1994) *Biochemistry 33*, 9523−9529.
13. McIntosh, J. M., Yoshikami, D., Mahe, E., Nielsen, D. B., Rivier, J. E., Gray, W. R., and Olivera, B. M. (1994) *J. Biol. Chem. 269*, 16733−16739.
14. Martinez, J. S., Olivera, B. M., Gray, W. R., Craig, A. G., Groebe, D. R., Abramson, S. N., and McIntosh, J. M. (1995) *Biochemistry 34*, 14519−14526.
15. Hu, S.-H., Gehrmann, J., Guddat, L. W., Alewood, P. F., Craik, D. J., and Martin, J. L. (1996) *Structure 4*, 417−423.
16. Guddat, L. W., Martin, J., Shan, L., Edmundson, A. B., and Gray, W. R. (1996) *Biochemistry 35*, 11329−11335.
17. Pardi, A., Galdes, A., Florance, J., and Maniconte, D. (1989) *Biochemistry 28*, 5494−5501.
18. Han, K.-H., Hwang, K.-J., Kim, S.-M., Kim, S.-K., Gray, W. R., Olivera, B. M., Rivier, J., and Shon, K.-J. (1997) *Biochemistry 36*, 1669−1677.
19. Stura, E., and Wilson, I. A. (1990) *Methods 1*, 38−49.
20. Matthews, B. W. (1968) *J. Mol. Biol. 33*, 491−497.
21. Otwinowski, Z. (1993) in *Proceedings of the CCP4 Study Weekend: Data Collection and Processing* (Sawyer, L., Isaacs, N., and Bailey, S., Eds.) pp 55−62, SERC Daresbury Laboratory, Warrington, U.K.
22. Minor, W. (1993) in *XDISPLAYF Program*, Purdue University, West Lafayette, IN.
23. Brünger, A. T. (1992) *X-PLOR (Version 3.1) Manual*, Yale University Press, New Haven, CT.

24. Fitzgerald, P. M. D. (1988) *J. Appl. Crystallogr. 21*, 273−278.
25. Miller, R., Gallo, S. M., Khalak, H. G., and Weeks, C. M. (1994) *J. Appl. Crystallogr. 27*, 613−621.
26. Blessing, R. H. (1989) *J. Appl. Crystallogr. 22*, 396−397.
27. Jones, T. A., Zou, J. Y., Cowan, S. W., and Kjeldgaard, M. (1991) *Acta Crystallogr. A 47*, 110−119.
28. Engh, R. A., and Huber, R. (1991) *Acta Crystallogr. A 47*, 392−400.
29. Sheldrick, G. M. (1993) *SHELXL93 A program for crystal structure refinement*, University of Göttingen, Göttingen, Germany.
30. Laskowski, R. A., MacArthur, M. W., Moss, D. S., and Thornton, J. M. (1993) *J. Appl. Crystallogr. 26*, 283−291.
31. Nicholls, A., Bharadwaj, R., and Honig, B. (1993) *Biophys. J. 64*, A116.
32. Kraulis, P. J. (1991) *J. Appl. Crystallogr. 24*, 946−950.
33. Luzzati, V. (1952) *Acta Crystallogr. 5*, 802−810.
34. Richardson, J. S. (1981) *Adv. Protein Chem. 34*, 167−339.
35. Srinivasan, N., Sowdhamini, R., Ramakrishnan, C., and Balaram, P. (1990) *Int. J. Pept. Protein Res. 36*, 147−155.
36. Kobayashi, Y., Ohkubo, T., Kyogoku, Y., Nishiuchi, Y., Sakakibara, S., Braun, W., and Go, N. (1989) *Biochemistry 28*, 4853−4860.
37. Ealick, S. E. (1997) *Structure 5*, 469−472.
38. Brünger, A. T. (1992) *Nature 355*, 472−475.
39. Cartier, G. E., Yoshikami, D., Gray, W. R., Luo, S., Olivera, B. M., and McIntosh, J. M. (1996) *J. Biol. Chem. 271*, 7522−7528.
40. Gray, W. R., Luque, F. A., Olivera, B. M., Barret, J., and Cruz, L. J. (1981) *J. Biol. Chem. 256*, 4734−4740.
41. Zafaralla, G. C., Ramilo, C. A., Gray, W. R., Karlstrom, R., Olivera, B. M., and Cruz, L. J. (1988) *Biochemistry 27*, 7102−7105.
42. Myers, R. A., Zafaralla, G. C., Gray, W. R., Abbott, J., Cruz, L. J., and Olivera, B. M. (1991) *Biochemistry 30*, 9370−9377.
43. Ramilo, C. A., Zafaralla, G. C., Nadasdi, L., Hammerland, L. G., Yoshikami, D., Gray, W. R., Kristipati, R., Ramachandran, J., Miljanich, G., Olivera, B. M., and Cruz, L. J. (1992) *Biochemistry 31*, 9919−9926.

BI9713052